

Matter radii of  $^{32-35}\text{Mg}$ 

R. Kanungo,<sup>1,\*</sup> A. Prochazka,<sup>2,3</sup> W. Horiuchi,<sup>2</sup> C. Nociforo,<sup>2</sup> T. Aumann,<sup>2</sup> D. Boutin,<sup>3</sup> D. Cortina-Gil,<sup>4</sup> B. Davids,<sup>5</sup> M. Diakaki,<sup>6</sup> F. Farinon,<sup>2,3</sup> H. Geissel,<sup>2</sup> R. Gernhäuser,<sup>7</sup> J. Gerl,<sup>2</sup> R. Janik,<sup>8</sup> B. Jonson,<sup>9</sup> B. Kindler,<sup>2</sup> R. Knöbel,<sup>2,3</sup> R. Krücken,<sup>7</sup> M. Lantz,<sup>9</sup> H. Lenske,<sup>3</sup> Y. Litvinov,<sup>2,10</sup> B. Lommel,<sup>2</sup> K. Mahata,<sup>2</sup> P. Maierbeck,<sup>7</sup> A. Musumarra,<sup>11,12</sup> T. Nilsson,<sup>9</sup> C. Perro,<sup>1</sup> C. Scheidenberger,<sup>2</sup> B. Sitar,<sup>8</sup> P. Strmen,<sup>8</sup> B. Sun,<sup>2,13</sup> Y. Suzuki,<sup>14,15</sup> I. Szarka,<sup>8</sup> I. Tanihata,<sup>16</sup> Y. Utsuno,<sup>17</sup> H. Weick,<sup>2</sup> and M. Winkler<sup>2</sup>

<sup>1</sup>*Astronomy and Physics Department, Saint Mary's University, Halifax, Nova Scotia B3H 3C3, Canada*

<sup>2</sup>*GSI Helmholtzzentrum für Schwerionenforschung, D-64291 Darmstadt, Germany*

<sup>3</sup>*Justus-Liebig University, D-35392 Giessen, Germany*

<sup>4</sup>*Universidad de Santiago de Compostela, E-15706 Santiago de Compostella, Spain*

<sup>5</sup>*TRIUMF, Vancouver, British Columbia V6T 2A3, Canada*

<sup>6</sup>*National Technical University, Athens, Greece*

<sup>7</sup>*Physik Department E12, Technische Universität München, D-85748 Garching, Germany*

<sup>8</sup>*Faculty of Mathematics and Physics, Comenius University, SK-84215 Bratislava, Slovakia*

<sup>9</sup>*Chalmers University of Technology, SE-412-916 Göteborg, Sweden*

<sup>10</sup>*Max-Planck-Institut für Kernphysik, Saupfercheckweg 1, D-69117 Heidelberg, Germany*

<sup>11</sup>*Universita' di Catania, I-95153 Catania, Italy*

<sup>12</sup>*INFN-Laboratori Nazionali del Sud, I-95123 Catania, Italy*

<sup>13</sup>*School of Physics and Nuclear Energy Engineering, Beihang University, 100191 Beijing, People's Republic of China*

<sup>14</sup>*Department of Physics, Niigata University, Niigata 950-2181, Japan*

<sup>15</sup>*RIKEN Nishina Center, RIKEN, Wako-shi, Saitama 351-0918, Japan*

<sup>16</sup>*RCNP, Osaka University, Mihogaoka, Ibaraki, Osaka 567 0047, Japan*

<sup>17</sup>*Japan Atomic Energy Agency, Tokai, Ibaraki 319-1195, Japan*

(Received 19 November 2010; published 9 February 2011)

The interaction cross sections of  $^{32-35}\text{Mg}$  at 900A MeV have been measured using the fragment separator at GSI. The deviation from the  $r_0A^{1/3}$  trend is slightly larger for  $^{35}\text{Mg}$ , signaling the possible formation of a longer tail in the neutron distribution for  $^{35}\text{Mg}$ . The radii extracted from a Glauber model analysis with Fermi densities are consistent with models predicting the development of neutron skins.

DOI: [10.1103/PhysRevC.83.021302](https://doi.org/10.1103/PhysRevC.83.021302)

PACS number(s): 25.60.Dz, 21.60.Cs, 21.10.Gv

The shell structure of nuclei has formed a fundamental basis for understanding their properties. As nuclei accumulate a large excess of neutrons, the conventional shell structure starts to show signs of mutation. Investigations of ground-state properties of neutron-rich nuclei are a key toward the search for the effects leading to the breakdown of the conventional shell structure. The matter radii of neutron-rich nuclei are one of the fundamental properties that constrain nuclear wave functions and carry crucial information on deformation, shell effects, and formation of neutron skins and halos [1].

In this Rapid Communication we report on the first determination of the matter radii of  $^{33-35}\text{Mg}$  in the  $N = 20$  island of inversion from a measurement of the interaction cross section. The results are consistent with development of neutron skins with  $^{35}\text{Mg}$  showing the possibility of a longer density tail.

The breakdown of the  $N = 20$  shell gap was observed through the low excitation energy of the  $2^+$  state in  $^{32}\text{Mg}$  [2]. Much effort has been devoted since then to the study of level schemes in attempting to understand this. The large  $B(E2)$  values deduced from the Coulomb excitation

measurements [3,4] were suggestive of  $^{32}\text{Mg}$  being a deformed nucleus. It should be noted here that the extraction of the deformation value ( $\beta$ ) in [3] is obtained under the assumption of a collective model. For a proper understanding of deformation in these nuclei, measured radii are important.

The level scheme of  $^{32}\text{Mg}$  from  $\beta$  delayed  $\gamma$  spectroscopy of  $^{32}\text{Na}$  [5] suggests that  $^{32}\text{Mg}$  is not an axially symmetric rotor. It is not a vibrational nucleus either. It was in fact discussed [6], based on a Skyrme-Hartree-Fock description, that this nucleus probably exhibits  $\gamma$  unstable deformation. A relativistic mean-field (RMF) calculation with three-dimensional angular momentum projection involving triaxial degrees of freedom [7] gives a ground state having  $\beta = 0.6$  and  $\gamma = 10^\circ$ . Density and radii from such models would be useful for comparison with the present data. Recently, a shape coexistent  $0^+$  state has been found in  $^{32}\text{Mg}$  [8].

The Monte Carlo shell model (MCSM) [9] has been considered to be fairly well suited to describe the levels in nuclei around the island of inversion. The predicted level scheme of  $^{32}\text{Mg}$  also does not show features of an axially symmetric rotor.

Mean-field models based on the Hartree-Fock (HF) or Hartree-Fock-Bogoliubov (HFB) approximations have been developed by several groups [10–12] for the neutron-rich

\*ritu@triumf.ca

Mg isotopes. Using a Skyrme force in the mean field, Terasaki *et al.* [10] predict  $^{36,38,40}\text{Mg}$  to be strongly deformed with varying deformations for the protons and neutrons. A Gaussian expansion method [12] with Gogny interaction suggests an extended neutron density tail in  $^{40}\text{Mg}$ . In calculations beyond a mean field [13], an interesting transition is observed from  $^{28-32}\text{Mg}$  showing shape coexistence to  $^{34}\text{Mg}$  with prolate deformation in the ground state.

The interaction cross section for  $^{20,22-25,27,29-32}\text{Mg}$  measured at 950A MeV with a C target indicates the development of neutron skins [14]. A measurement of the reaction cross section [15] at much lower energies using an active target silicon detector shows a very large cross section for  $^{35}\text{Mg}$ . This measurement relies on detecting all reaction products. Without  $4\pi$  coverage, missing out-of-plane reaction event detection may cause uncertainty. The effects of channeling in silicon detectors also introduce a larger uncertainty in the extracted cross sections. Furthermore, as discussed in Ref. [15] assumptions need to be made to disentangle the one-neutron removal events, the difficulty of which increases as one moves to more weakly bound nuclei. The method of transmission of the unreacted secondary beam on the other hand is a reliable and well-established way to measure the interaction cross section.

We measured the interaction cross section of neutron-rich Mg isotopes in order to extract the root mean square (rms) matter radius ( $R_{\text{rms}}^m$ ). The total interaction cross section for the reaction in the target is given by  $\sigma_I = -t \ln(R_{\text{out}}/R_{\text{in}})$ , with the transmission ratio  $R_{\text{in}} = N_{\text{in}}^i/N_{\text{in}}^f$ , where  $N_{\text{in}}^i$  and  $N_{\text{in}}^f$  are the numbers of  $^A\text{Mg}$  before and after the target, respectively,  $R_{\text{out}}$  is the same but for an empty target, and  $t$  is the number of target nuclei per unit area.

The experiment was performed using the fragment separator (FRS) at GSI, Darmstadt [16]. Figure 1 sketches the experimental setup. The secondary beams of neutron-rich  $^{32-35}\text{Mg}$  isotopes were produced through the fragmentation of a  $^{48}\text{Ca}$  primary beam ( $10^9/\text{spill}$ ) on a  $6.347\text{ g/cm}^2$  thick Be target. The nuclei produced were then separated and identified using the first half of the FRS. The time of flight (TOF) was measured between two plastic scintillator detectors placed at the first dispersive focus (F1) and the dispersive midplane (F2). The reaction target was placed at the dispersive midplane. Time-projection chamber (TPC) tracking detectors placed at F2 before the target were used for beam tracking. The energy loss ( $\Delta E$ ) of the incoming mixture of isotopes was measured

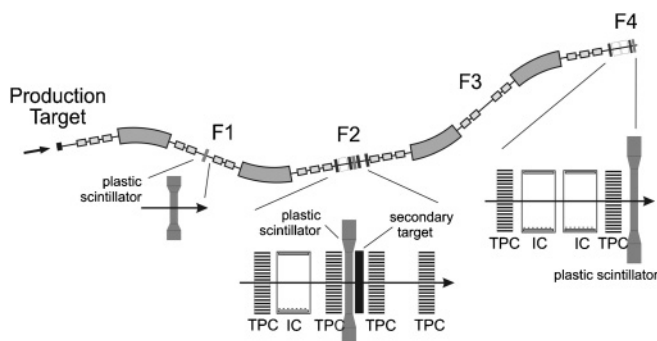


FIG. 1. Schematic layout of the experiment.

using a multisampling ionization chamber (MUSIC) placed before the reaction target. The incoming  $^A\text{Mg}$  isotopes were identified and counted event by event using these detectors. The atomic number  $Z$  of the beam was identified using the energy-loss information. The position of the beam at the target, the TOF, and the magnetic rigidity ( $B\rho$ ) provide a measure of the  $A/Q$  ratio of the beam.

Carbon and  $(\text{CH}_2)_n$  reaction targets were mounted on a movable target ladder having an empty target frame position as well. The carbon target thickness was  $4.046\text{ g/cm}^2$  while that of the  $(\text{CH}_2)_n$  target was  $3.988\text{ g/cm}^2$ . Two other thicknesses of carbon targets, namely  $2.523$  and  $7.062\text{ g/cm}^2$ , were used for the  $^{33}\text{Mg}$  beam to check if there is any loss due to multiple scattering in deriving the interaction cross sections. The uncertainty in the target thicknesses varied from  $0.4\%$  to  $1.2\%$ .

The interaction cross section is measured based on the method of transmission where one needs to identify and count the number of unreacted  $^A\text{Mg}$  isotopes after the reaction target. The separation and identification were done by using the second half of the fragment separator as an analyzer. It was set to transport the unreacted  $^A\text{Mg}$  to the final achromatic focus F4. The  $Z$  and  $A/Q$  identifications were done by the  $B\rho-\Delta E$ -TOF method. The TOF was measured using plastic scintillator detectors placed at F2 and F4. The tracking using two TPC detectors at F4 provides the position and angle. Two MUSICs were placed at F4 for a complete understanding of the identification efficiency. Events that were observed to be consistent with  $Z = 12$  in either MUSIC were counted as unreacted events. To account for losses occurring due to reactions in other materials in the setup, data were also collected with an empty target frame.

Transmission through the FRS was studied by varying the selection of position and angle openings both in the  $X$  and

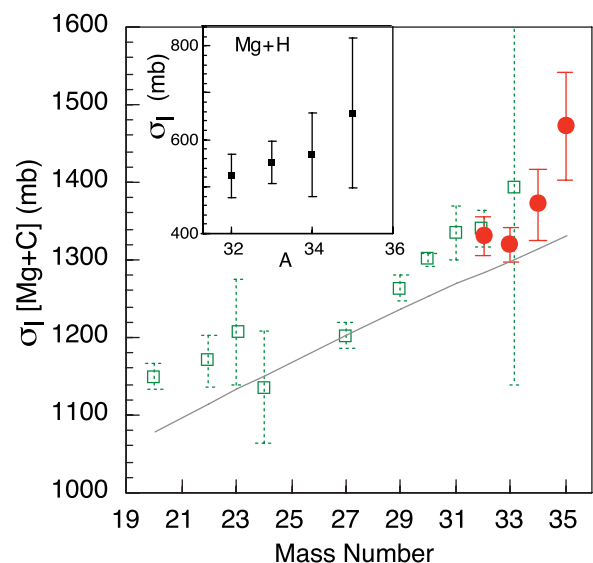


FIG. 2. (Color online) The measured interaction cross section for  $^{32-35}\text{Mg}$  (circles) on a C target and (inset) on H [derived from a  $(\text{CH}_2)_n$  target and C target data]. The open squares show data from Ref. [14]. The line (normalized close to stability) shows the monotonic increase expected from an  $A^{1/3}$  dependence on radii.

$Y$  directions. The phase space was chosen from this study to select the region with a constant transmission for each data set. The sequence of target and no-target data was repeated alternately several times for a particular target and beam combination to ensure that there was no systematic variation in transmission due to changes of the magnetic fields.

The backgrounds from  $Z = 11$  and  $Z = 13$  ions in the selection of incident beam events were  $\sim 0.2\%$  and  $0.02\%$ , respectively. The dominant background contribution to the incoming beam selection is from the mass identification. This was estimated individually for each sequence of runs with and without a target and was included in the final uncertainty estimation of the cross section. For the  $^{33}\text{Mg}$  beam the background level was  $0.6\%–0.9\%$  when the phase space of the incoming beam was restricted by small slit openings at F1. By using wider slit openings, a larger contamination level was found ( $\sim 3\%–5\%$ ).

The interaction cross section for  $^{33}\text{Mg}$  with different target thicknesses is consistent within the uncertainty, showing the measured values to be devoid of any thickness-dependent

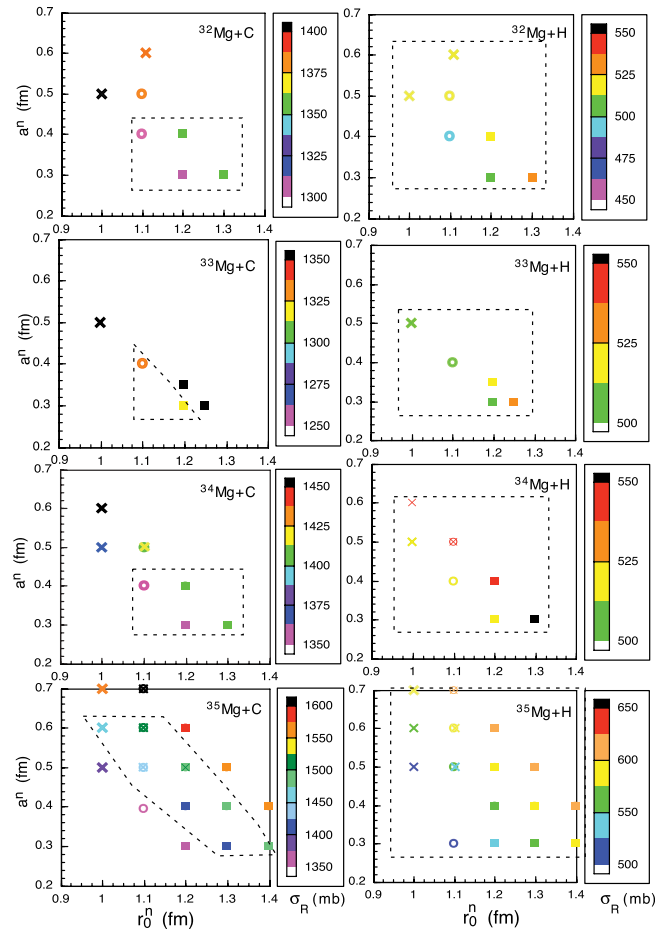


FIG. 3. (Color online) The calculated reaction cross sections for  $^A\text{Mg} + \text{C}$  and  $^A\text{Mg} + \text{H}$  are shown by the colored bar plotted as a function of the neutron density parameters  $r_0^n$  and  $a^n$ . The three different symbols represent calculations for different density profiles. Cross:  $r_0^p = 0.97$  fm and  $a^p = 0.5$  fm; circle:  $r_0^p = 1.09$  fm and  $a^p = 0.4$  fm; and square:  $r_0^p = 1.18$  fm and  $a^p = 0.3$  fm. The dotted line encloses points consistent with the  $1\sigma$  uncertainty of the data.

effect. Figure 2 shows the weighted average of different data sets of the measured cross sections for  $^{32-35}\text{Mg}$ . The increase in cross section of  $^{32-35}\text{Mg}$  compared to the solid line (Fig. 2) shows the development of a neutron skin. The cross section of  $^{35}\text{Mg}$  shows a larger deviation possibly showing the development of a more diffuse neutron distribution for  $^{35}\text{Mg}$ . This might be expected from its small one-neutron separation energy.

The data are interpreted in the Glauber model [17,18] using the phase-shift function that includes higher-order terms missing in the conventional optical limit approximation. The proton-neutron and proton-proton (neutron-neutron) interactions are distinguished and the parameters of the profile function employed are given in Ref. [18]. In order to extract the rms radii, we consider a Fermi density for protons and neutrons of  $\bar{\rho}(r)^i = \rho_0^i / \{1 + \exp[(r - R^i)/a^i]\}$ , where  $R^i = r_0^i A^{1/3}$  with the index  $i$  denoting protons ( $p$ ) or neutrons ( $n$ ).

For the proton density we consider several sets of  $r_0^p$  and  $a^p$  consistent with the point proton radius of  $^{24-26}\text{Mg}$ . The parameters  $r_0^n$  and  $a^n$  were varied to find the combinations that reproduced the measured interaction cross sections for  $^A\text{Mg} + \text{C}$  and  $^A\text{Mg} + \text{H}$  with the condition that  $r_0^n \geq r_0^p$  and  $a^n \geq a^p$  for each set of  $r_0^p$  and  $a^p$ . The calculated cross sections are shown in Fig. 3 as a function of  $r_0^n$  and  $a^n$  and in Fig. 4 as a function of the  $R_{\text{rms}}^m$ .

The study shows that the interaction cross section can be slightly different for different density parameters  $r_0$  and  $a$ , giving nearly identical  $R_{\text{rms}}^m$ . This shows the importance of using a functional form closest to a realistic density profile. To this end, we have adopted a Fermi density profile instead of a harmonic oscillator one.

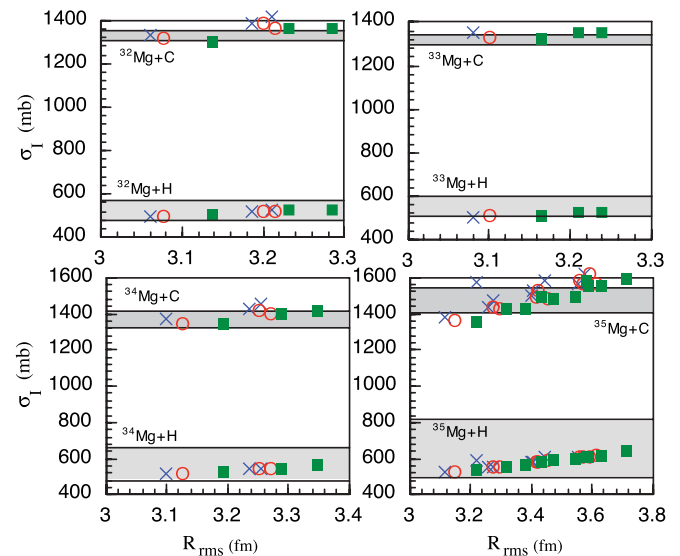


FIG. 4. (Color online) The shaded horizontal bars show the measured interaction cross sections of  $^A\text{Mg}$  with C and H targets as labeled in each figure. The three different symbols show the calculated reaction cross sections for three different proton density profiles with correspondingly different neutron densities. Cross:  $r_0^p = 0.97$  fm and  $a^p = 0.5$  fm; circle:  $r_0^p = 1.09$  fm and  $a^p = 0.4$  fm; and square:  $r_0^p = 1.18$  fm and  $a^p = 0.3$  fm.

TABLE I. Measured interaction cross sections and the rms [ $R_{\text{rms}}^m(\text{ex})$ ] matter radii for  $^{32-35}\text{Mg}$  extracted from them are compared with the HF and RMF predictions.

Isotope	$\sigma_I^C$ (mb)	$\sigma_I^H$ (mb)	$R_{\text{rms}}^m(\text{ex})$ (fm)	HF [6] <sup>a</sup> (fm)	RMF [20] (fm)
$^{32}\text{Mg}$	1331(24)	523(47)	$3.17 \pm 0.11$	3.20	3.21
$^{33}\text{Mg}$	1320(23)	552(45)	$3.19 \pm 0.03$	3.23	3.26
$^{34}\text{Mg}$	1372(46)	568(90)	$3.23 \pm 0.13$	3.26	3.33
$^{35}\text{Mg}$	1472(70)	657(160)	$3.40 \pm 0.24$	3.30	3.38

<sup>a</sup>The values are read from [6].

It is interesting to observe that for  $^{32-34}\text{Mg}$ , the diffuseness of the neutron density is close to that of the protons for any choice of  $a^p$ , while for  $^{35}\text{Mg}$  the observed cross sections allow a longer neutron density tail. This shows an indication of a possible onset of halo formation for Mg isotopes at and beyond  $N = 23$ . In the future it would be important to determine the proton density of these isotopes to quantify more accurately the neutron skin thickness.

The neutron-rich Mg isotopes under discussion have highly mixed ground-state configurations [19]. In the island of inversion around  $N = 20$ , a clear distinction between core nucleon and valence nucleon is not possible, so a decoupled core + neutron picture is not appropriate for these nuclei. We therefore consider the core + neutron few-body Glauber model to be an inappropriate way to interpret the interaction cross section of these nuclei.

The  $R_{\text{rms}}^m$  reported here are from consistent descriptions of interaction cross sections of  $^A\text{Mg}$  with both C and H (Fig. 4) using different density profiles for the protons. Table I summarizes the extracted radii for the various isotopes. The larger uncertainty in the radius of  $^{32}\text{Mg}$  in Table I compared to Ref. [14] ( $3.12 \pm 0.05$  fm) stems from our approach to include the effect of uncertainty from different density profiles of the protons. The matter radii predicted

[20] by the RMF theory with NL-SH force and mean-field predictions with [6,21] the Skyrme III interaction are also shown. Both models are consistent with the experimental radii within the uncertainties. The measured interaction cross sections are expected to motivate further development of models for a more detailed understanding of deformation and the development of neutron skins.

It may be mentioned here that Ref. [15] provides only information on reduced strong absorption radii based on a simple phenomenological model. From this description (based on  $r_0 A^{1/3}$ ) assuming a sharp surface, the approximate rms radii obtained with the  $r_0^2$  values listed in Ref. [15] are significantly smaller than the radii found through a Glauber model analysis of the high-energy interaction cross section. It has been known that such phenomenological models are not well suited for a detailed quantitative description on the structure but could be used to understand a general trend of systematics. The work reported here provides the first measurement of rms matter radii of neutron-rich Mg isotopes which can be utilized for comparison with nuclear structure models. Furthermore, the availability of density distributions from structure models in the future can be directly used for comparison with the measured cross sections.

In summary, the interaction cross sections of  $^{32-35}\text{Mg}$  were measured using C and  $\text{CH}_2$  targets at  $\sim 900$  A MeV. The cross section for  $^{35}\text{Mg}$  is found to be slightly larger than the  $r_0 A^{1/3}$  trend, suggesting the possibility of a modest extension of the neutron density diffuseness. The measured rms matter radii extracted from the data show the development of neutron skins.

The authors acknowledge the support of the GSI accelerator staff and the FRS technical staff for an efficient running of the experiment. The support from Natural Sciences and Engineering Research Council of Canada (NSERC) for this work is gratefully acknowledged. This work was supported by the BMBF under Contract No. 06MT238 and by the DFG Cluster of Excellence *Origin and Structure of the Universe*.

- 
- [1] I. Tanihata *et al.*, *Phys. Rev. Lett.* **55**, 2676 (1985).  
[2] D. Guillemaud-Mueller *et al.*, *Nucl. Phys. A* **426**, 37 (1984).  
[3] T. Motobayashi *et al.*, *Phys. Lett. B* **346**, 9 (1995).  
[4] B. V. Pritychenko *et al.*, *Phys. Lett. B* **461**, 322 (1999).  
[5] V. Tripathi *et al.*, *Phys. Rev. C* **77**, 034310 (2008).  
[6] T. Otsuka, *Nucl. Phys. A* **616**, 406c (1997).  
[7] J. M. Yao *et al.*, *Phys. Rev. C* **79**, 044312 (2009).  
[8] K. Wimmer *et al.*, *Phys. Rev. Lett.* **105**, 252501 (2010).  
[9] Y. Utsuno, T. Otsuka, T. Mizusaki, and M. Honma, *Phys. Rev. C* **64**, 011301(R) (2001).  
[10] J. Terasaki *et al.*, *Nucl. Phys. A* **621**, 706 (1997).  
[11] P. D. Steveston *et al.*, *Phys. Lett. B* **545**, 291 (2002).  
[12] H. Nakada, *Nucl. Phys. A* **808**, 47 (2008).  
[13] R. Rodríguez-Guzmán *et al.*, *Nucl. Phys. A* **709**, 201 (2002).  
[14] T. Suzuki *et al.*, *Nucl. Phys. A* **630**, 661 (1998).  
[15] A. Khouaja *et al.*, *Nucl. Phys. A* **780**, 1 (2006).  
[16] H. Geissel *et al.*, *Nucl. Instrum. Methods Phys. Res. B* **70**, 286 (1992).  
[17] B. Abu Ibrahim and Y. Suzuki, *Phys. Rev. C* **61**, 051601(R) (2000).  
[18] B. Abu Ibrahim, W. Horiuchi, A. Kohama, and Y. Suzuki, *Phys. Rev. C* **77**, 034607 (2008).  
[19] R. Kanungo *et al.*, *Phys. Lett. B* **685**, 253 (2010).  
[20] Z. Ren *et al.*, *Phys. Lett. B* **380**, 241 (1996).  
[21] N. Fukunishi, T. Otsuka, and I. Tanihata, *Phys. Rev. C* **48**, 1648 (1993).